Applied Physics A (2019) 125:98
https://doi.org/10.1007/s00339-019-2398-y

Applied Physics A
Materials Science & Processing

Fractal and multifractal analysis of In-doped ZnO thin films deposited on glass, ITO, and silicon substrates

Koushik Ghosh[1] · R. K. Pandey[1]

Received: 13 November 2018 / Accepted: 9 January 2019 / Published online: 12 January 2019
© Springer-Verlag GmbH Germany, part of Springer Nature 2019

Abstract

Indium-doped zinc oxide (IZO) thin films have been deposited on glass (IZO/glass), ITO (IZO/ITO), and silicon (IZO/Si) substrates using sol–gel spin coating method. Glancing angle X-ray diffraction has been used to verify phase purity, average grain size, and microcrystalline stress of the annealed films. Effect of substrates on surface morphology is explicitly investigated using the conventional statistical techniques along with nonlinear fractal and multifractal geometrical analysis. The root-mean-square surface roughness value is the lowest in IZO/glass films and increases in IZO/ITO films and the highest in IZO/Si films. Fractal and multifractal formalism acts as a scale-independent microscopic analytical tool for surface analysis. All IZO films show fractal and multifractal behaviour. The fractal parameters such as fractal dimensions and Hurst exponents are different for films deposited on different substrates and, thus, able to characterize surface morphology precisely. Hurst exponent values of IZO films indicate that although IZO/Si films have highest vertical roughness, it has strongly correlated (highest self-similarity) surface morphology than other two films deposited on glass and ITO substrates. Inhomogeneity in scaling exponents could be better understood with the help of multifractal formalism. The difference of fractal dimensions in all IZO films deposited on glass, ITO, and Si substrates is very small (almost close to zero). Therefore, there is very little multifractality exist in those film surfaces. Width of multifractal spectrum is the largest in IZO/Si and the smallest (also similar) in IZO/ITO and IZO/glass films, indicating that multifractallity in IZO/Si film is more prominent. A quantitative information about the surface morphology has been provided by inferring multifractal parameters. Detailed fractal and multifractal formalism of surface morphology may find its importance in understanding various surface-based device fabrication and performances.

1 Introduction

Science and technology of oxide semiconductors having a wide bandgap have seen intense progresses since last few decades due to utility of them in optoelectronic devices such as short wavelength lasers, LEDs, etc. and in low-cost energy-harvesting technology [1–3]. Among various wide band-gap compound semiconductors zinc oxide (ZnO) is a low cost and nontoxic one. It has potential to be used as transparent conducting oxide (TCO) electrodes in various optoelectronic devices [4, 5]. ZnO has been also used to fabricate super hydrophobic [6] and self-cleaning [7] coatings.

Doping of group III elements (Al/Ga/In) in ZnO enhances transparency, bandgap, etc. [8, 9]. Therefore, In-doped ZnO thin films were studied for their various structural, optical, and electrical properties by many researchers [10–12].

Surface plays a major role in TCO materials as their transparency and electrical transport properties are greatly influenced by more and more homogeneous and defect free surfaces. Wettability and self-cleaning properties also depend on complex surface architecture [13, 14]. Hence, precise characterization of In-doped ZnO thin-film surface morphology deposited on various substrates is needful. Among many surface imaging techniques, atomic force microscopy (AFM) is a proficient non-destructive technique to obtain surface micrographs [15]. AFM images are generally quantified by many researchers using the conventional average roughness, root-mean-square (RMS) roughness, skewness, and kurtosis analysis. These conventional parameters are not free from measuring instruments inherent limitations [16, 17]. On the other hand, fractal and multifractal calculations are scale-independent methods for surface morphology characterization [18].

✉ Koushik Ghosh
koushik.resh@gmail.com

[1] Department of Pure and Applied Physics, Guru Ghasidas Vishwavidyalaya, Bilaspur 495009, India

A few researchers in the past have done fractal and multifractal analysis of thin-film surface micrographs. Raoufi [19] found that fractal dimension can quantify surface morphology while analysing ITO thin films on glass substrates using power spectral density (PSD)-based fractal analysis method. Dallaeva et al. [20] have observed that fractal dimension can play crucial role in surface topography measurement of AlN thin films on Al_2O_3 substrates. Fractal characteristics of transition-metal oxide thin films (ZnO, TiO_2, Al_2O_3, WO_3, and Nb_2O_5) were investigated by Chen et al. [21]. Fractal analysis of conducting polypyrrole thin films using PSD, perimeter-area and box-counting methods shown that fractal dimension (FD) increases upon increasing film thickness [22]. Interdependence of FD with different shape and size of Cu was observed in Cu_2O/Cu composites [23]. Gas-sensing performance of SnO_2 thin films was found to be correlated with fractal parameters which were computed from scanning electron microscopic (SEM) images using box-counting technique [24]. Fractal patterns of oxide nanoparticles on flat surfaces can generate super hydrophilicity [25]. A correlation between super hydrophobicity and the PSD was observed by Awada et al. [26]. Effect of fractal parameters on rough surface's wettability property was also investigated by Jain et al. [27]. PSD-based fractal methodology was applied to understand nanostructure formation and wettability property in ion-treated silver (Ag) thin films [28]. In nanostructured LiF films, FD is inversely proportional to the substrate temperature in the course of deposition [29]. Higuchi's algorithm was used to compute fractal dimension of reactive magnetron sputtered Ag–Cu thin films and complexity of surface morphology was understood in terms of fractal behaviour [30]. Yadav et al. [31] observed correlation between deposition angle, fractal dimension, and grain size in atom beam-sputtered ZnO thin films. Fractal analysis was done on the AFM images of ion-bombarded Si surfaces and it was observed that roughness exponent is proportional to the ion fluence [32]. Fractal dimensions were computed for ion-treated Au nanostructures and it was observed that FDs do not follow any trend with ion fluence [33]. Multifractallity of nanostructured gold (Au) thin films was investigated using multifractal detrended fluctuation analysis (MFDFA) method [34]. In swift heavy ion (SHI) irradiated BaF_2 thin films, fractal and multifractal parameters do not follow any trend with ion fluence, although average roughness decreases monotonically with increasing ion fluence [35]. In SHI irradiated CaF_2 thin films, multifractal analysis indicate that surface complexity first decreases and then increases with increasing ion beam fluence [36]. Multifractallity of thin-film surface increases with increasing film thickness, and, thus, complexity of surface increases as observed from multifractal characterization of AFM images of Al-doped ZnO [37], silver [38], and LiF [39] thin films. Multifractal analysis of LiF thin films deposited at different substrate temperature using electron beam evaporation method had shown that multifractallity increases as the substrate temperature increases, and thus, inhomogeneous surfaces developed [40].

Although some works regarding fractal and multifractal analysis of thin-film surfaces are done, but, to the best of our knowledge, no one have done a fractal and multifractal analysis of In-doped ZnO thin-film surfaces deposited on different substrates using sol–gel spin coating method. Effect of glass, ITO, and silicon substrates to the complexity of In-doped ZnO thin-film surface morphology are investigated explicitly using fractal and multifractal analysis along with the conventional statistical analysis.

2 Experimental details

2.1 Thin-film deposition

In this work, indium-doped ZnO thin films were deposited on glass, ITO, and Si substrates using sol–gel spin coating technique. Solvent, precursor compounds, and stabilizer were of electronic grade and brought from Sigma-Aldrich. All these chemicals were used without further purification. The solution was prepared for spin coating by dissolving zinc acetate dehydrate ($Zn(CH_3COO)_2 \cdot 2H_2O$) [ZAD] in 2-methoxy ethanol ($C_3H_8O_2$). Mono-ethanolamine (MEA, C_2H_7NO) was mixed in the solution to stabilize the reaction. Total solution concentration was preserved at 0.4M and MEA to ZAD molar ratio was kept at 1.0. Indium nitrate hydrate [$In(NO_3)_3$, xH_2O] was taken as a source of Indium dopant in the solution. Indium-doping concentration was fixed at 2 at%. The solution was stirred for 1 h at 50 °C using a magnetic stirrer to acquire a transparent solution. The solution was aged at room temperature for 48 h to obtain gel with needed viscosity. Glass, ITO, and silicon substrates were cleaned with acetone, methanol, and deionized water using ultrasonicator. Then those substrates were dried by blowing air and heating in air at 120 °C for 10 min. Thin films were then deposited on glass, ITO, and silicon substrates using a spin coater at a spinning rate of 3000 RPM for 30 s, including an accelerating time of 5 s. Deposited thin films were baked on a hot plate at 120 °C for 10 min to remove organic residuals. To obtain films of desired thickness, entire process was repeated ten times. Deposited and baked films were kept in a furnace to anneal them at 500 °C for 2 h. Annealed In-doped ZnO thin films (IZO) deposited on glass, ITO, and Si substrates are named as, respectively, IZO/glass, IZO/ITO, and IZO/Si.

2.2 Characterization techniques

Structural and phase purity characterization of IZO thin films were done using a 9 KW Rigaku SmartLab X-ray diffractometer. Glancing angle XRD spectra was taken using Cu K_α radiation having wavelength of 0.154 nm. Operating voltage and current of X-ray tube were maintained at, respectively, 45 kV and 200 mA. A Shimadzu scanning probe microscope (SPM 9600) was used to take surface micrographs of the annealed IZO thin films. In dynamic noncontact mode (10×10 μm^2), surface micrographs were acquired using a Si_3N_4 pyramidal tip. AFM images used for fractal and multifractal analysis were digitized in 256×256 pixels.

3 Results and discussion

3.1 Effect of substrates on structural properties

Crystalline structure and phase purity have been studied using glancing angle X-ray diffraction (GAXRD). GAXRD spectra of IZO films on glass, ITO, and Si substrates are shown in Fig. 1. All prominent characteristic planes for IZO thin films are indexed in this figure, and they are (100), (002), (101), (102), (110), (103), (200), (112), and (201). XRD patterns of IZO thin films deposited on three different substrates match with the hexagonal wurtzite pattern of JCPDS: 036-1451 [41]. No other peaks corresponding to indium and its oxides have been observed in XRD patterns which indicate the deposition of phase pure hexagonal wurtzite IZO films on glass, ITO, and Si substrates. Williamson–Hall (W–H) plots [42] of XRD spectrum have been used to calculate microcrystalline stress and average grain size of IZO films. A detailed methodology for W–H plot has been described in a previously published paper [43]. Figure 2 depicts W–H plots of IZO films. Calculated values of average grain size and microcrystalline stress from these plots are given in Table 1. Average grain size is maximum (22.03 nm) in films deposited on Si substrates and minimum in films deposited on glass (13.91 nm) and ITO (14.30 nm) substrates. The average grain size does not have much difference in case of IZO films deposited on glass and ITO substrates, whereas IZO thin films on Si substrates have higher average grain size because of the wrinkle formation at surface (as a result of this mounded surface appears) as could be seen in AFM image shown in the next section. Kumar et al. [44] also observed that the ZnO films deposited on Si substrates have higher average grain size than those deposited on glass substrates. The microcrystalline stress of IZO films deposited on all the three substrates is found to be compressive in nature. The

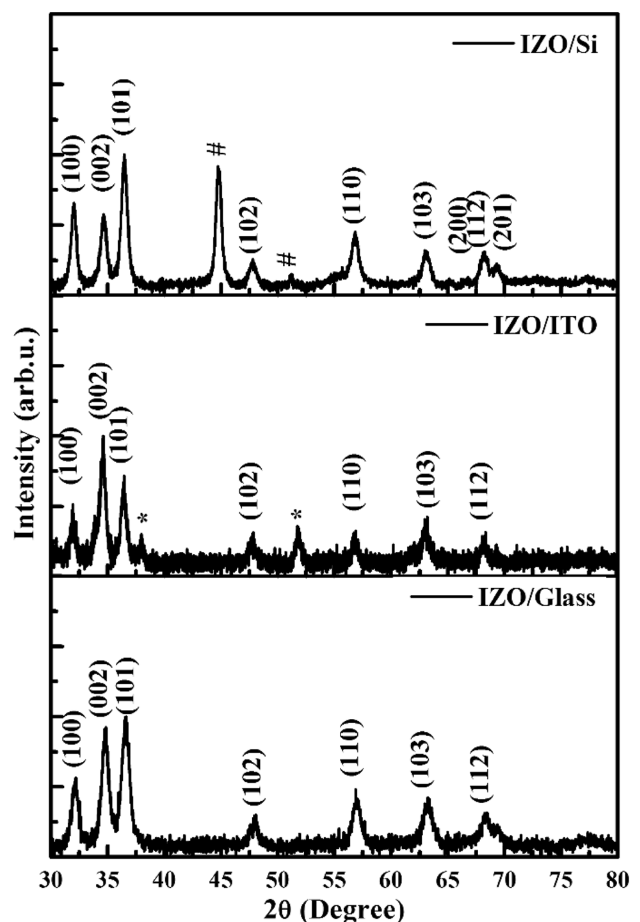

Fig. 1 XRD spectra of IZO thin films deposited on glass, ITO, and Si substrates (* and # marked peaks are substrate peaks)

reason behind this compressive nature of stress may be due to creation of large number of oxygen vacancy and zinc interstitials due to indium doping. The value of it is the highest in films deposited on Si substrate (− 0.676 GPa) and the lowest in films on ITO substrates (− 0.038 GPa), and in glass substrates, it is − 0.347 Gpa. Lattice and thermal expansion coefficient mismatch plays a crucial role in introduction of residual stress in thin films [45]. However, in the present case, these are not dominant factors, because if it is so, then glass and ITO should have highest residual stress [46]. Maximum residual stress may be understood in terms of maximum oxygen stoichiometry deterioration in case of Si substrates by the formation of its oxide at the junction during annealing of the films. Similar higher residual stress in ZnO films deposited on Si substrates than on glass substrates was observed by Ozen et al. [47]. However, further detailed experimental investigation is necessary to find out the origin of compressive stress and variation of it.

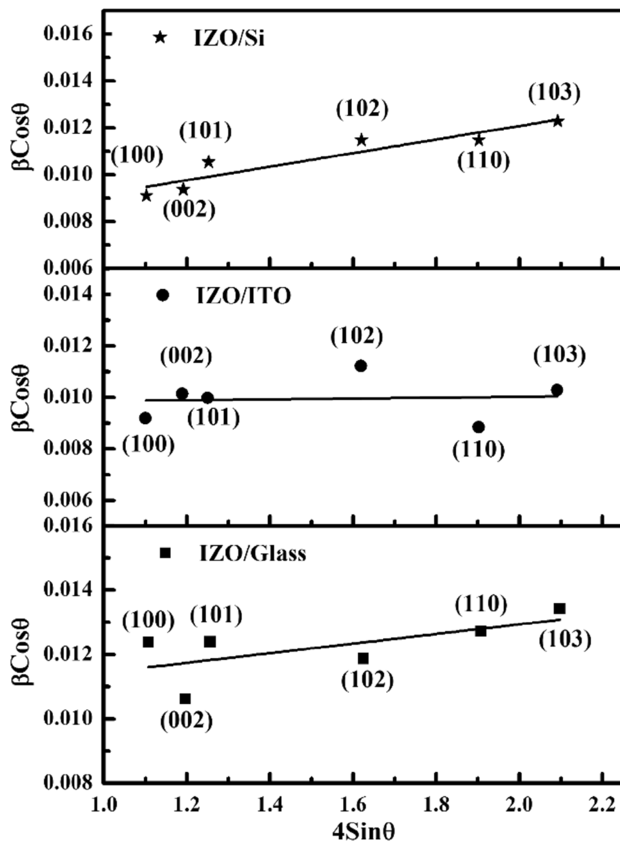

Fig. 2 Williamson–Hall plots of IZO thin films deposited on glass, ITO, and Si substrates (straight lines are linear fit to the data)

Table 1 Average grain size and microcrystalline stress of In-doped ZnO thin films on glass, ITO, and Si substrates

Sample name	Average grain size, D (nm)	Microcrystalline stress, σ (GPa)
IZO/glass	13.91	−0.347
IZO/ITO	14.30	−0.038
IZO/Si	22.03	−0.676

3.2 Effect of substrates on surface morphology

AFM images in Fig. 3 show surface morphology of IZO thin films deposited on three different substrates. Columnar grains at surface present in IZO/glass and IZO/ITO films where wrinkled surface formed in IZO/Si films. The average roughness and RMS roughness values of IZO films deposited on Si substrates are much higher than the films deposited on glass and ITO substrates (Table 2). RMS roughness profiles of AFM images are compared in Fig. 4a. It indicates prominent wrinkle formation on the IZO/Si film surface. Height distribution at the surface of IZO/glass film is very sharp, whereas, in IZO/FTO and IZO/Si, it is wider than the former as shown in Fig. 4b. Surface instability causes deformation at surface due to stress relaxation during the evaporation of solvent above boiling point, and thus, wrinkle formation took place [48, 49] It has been observed in XRD results that the highest compressive stress has been developed in IZO films on Si substrate. This compressive stress might have induced volumetric strain, and thus, wrinkles are formed which yielded large surface roughness in IZO/Si films [50]. Surface of polycrystalline ITO substrates (1.8 nm) has higher roughness than glass (0.5 nm); therefore, bigger grains are formed during deposition and crystallization; thus, IZO/ITO films have higher roughness than IZO/glass films. Symmetry of the surface could be understood in terms of skewness (R_{sk}) and kurtosis (R_{ku}) of the AFM images [51]. The value of skewness was smaller for films deposited on glass substrate and increased in case of ITO and Si substrates. The value of it is the highest in films deposited on Si substrates. Smaller skewness values represent more planner surfaces. Kurtosis value is the highest for the films deposited on ITO substrates which means that the surface has more peaks than valleys [52]. Kurtosis value is the smallest for the IZO films deposited on glass substrates. Therefore, the films deposited on glass substrates are flatter than others. However, spatial distribution of mass at the surface could not be understood precisely with these symmetry parameters. All the above-mentioned parameters come under the first-order statistics [53]. The first-order statistics or the height distribution function and parameters derived using this have certain limitations. It can only describe statistical mass distribution of a surface at individual positions. However, it cannot find correlation between those individual positions. Simply, one can say that the first-order statistics fails to find spatial self-similarities in surfaces having different surface texture and interface width. Therefore, to differentiate between different spatially organised surfaces, one needs to correlate surface heights.

3.2.1 Correlation length, fractal dimension, and Hurst exponent

The correlation of surface heights can be characterized in terms of correlation functions [39]. There are two forms of correlation functions, such as autocorrelation function (ACF) and height–height correlation function (HHCF). However, they provide similar information about a surface. The autocorrelation function has been usually derived from height profile $h(i,j)$ of $N_p \times N_p$ no. of points along the first scan direction as follows [35]:

$$A_c(r) = \frac{1}{2N_p\left(N_p - m\right)A_0} \sum_{j=1}^{N_p} \sum_{i=1}^{N_p - m} h(i+m,j)h(i,j), \quad (1)$$

where $h(i,j)$ is the height profile from the first scan direction, r is the distance between two points along the first scan

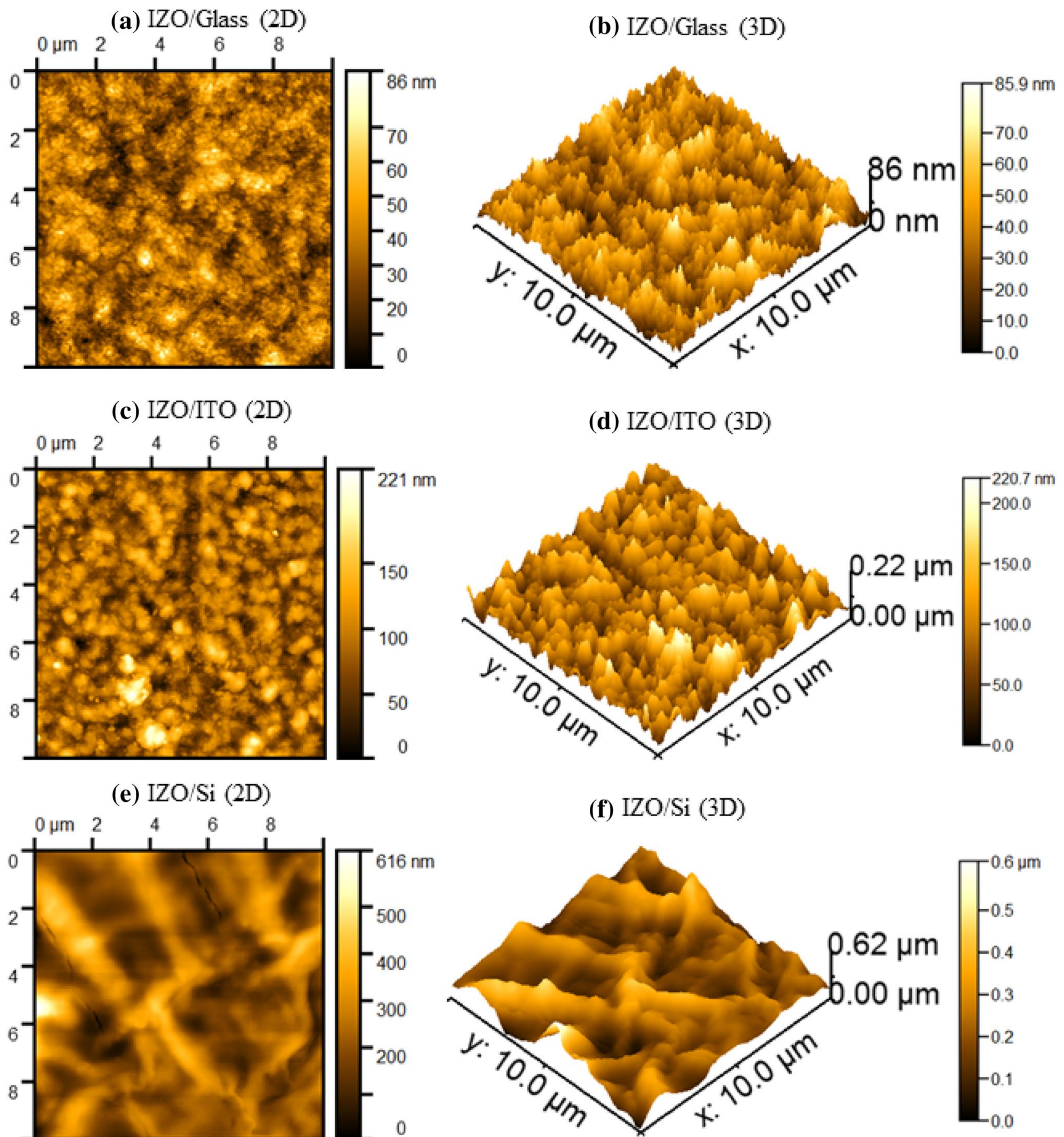

Fig. 3 Two- and three-dimensional AFM images of IZO thin films deposited on glass, ITO, and Si substrates

Table 2 Roughness parameters calculated from AFM images of In-doped ZnO thin films deposited on glass, ITO, and Si substrates

Sample name	Average roughness (R_a) (nm)	RMS roughness (R_q) (nm)	Skewness (R_{sk})	Kurtosis (R_{ku})
IZO/glass	8.62	10.96	0.42	0.34
IZO/ITO	22.16	28.55	0.64	0.97
IZO/Si	62.71	79.98	0.70	0.70

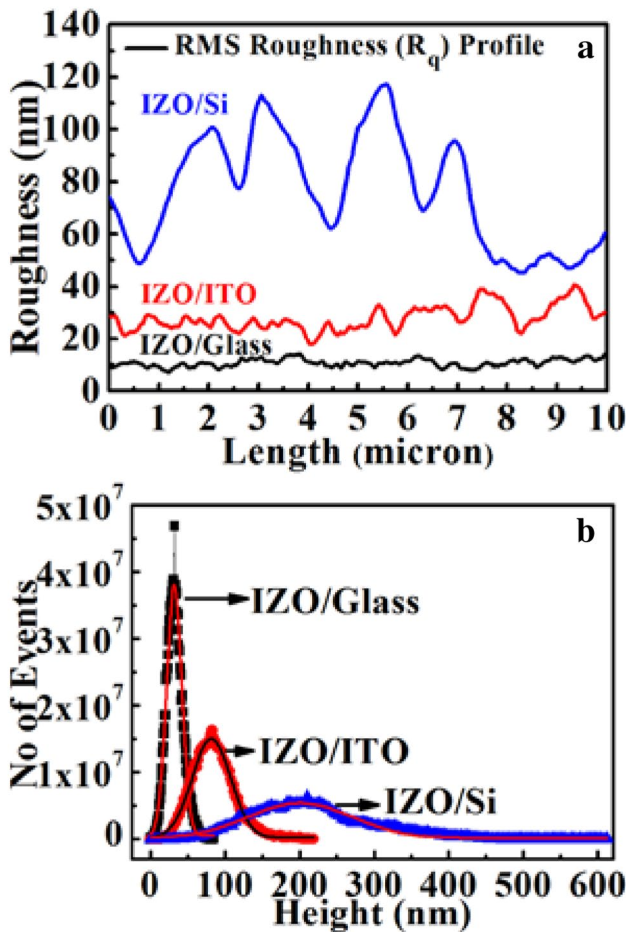

Fig. 4 **a** RMS roughness profiles and **b** Height distribution curves obtained from AFM images of IZO thin films deposited on glass, ITO, and Si substrates

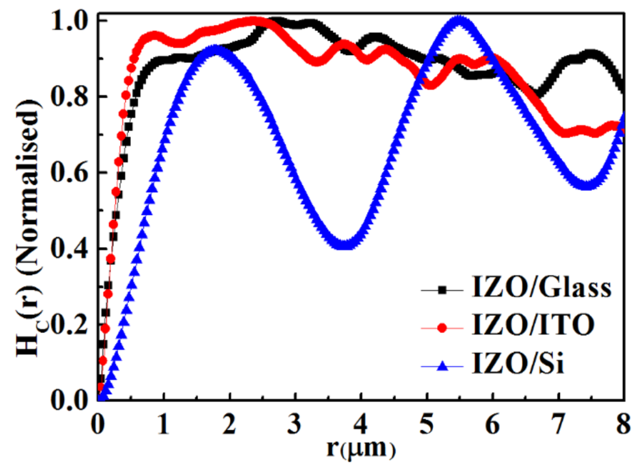

Fig. 5 Height–Height correlation functions calculated from AFM images of IZO thin films deposited on glass, ITO, and Si substrates

direction for which the correlation between pixels is calculated, N_p is the no. of pixels taken care of in the calculation, m is number of pixels used in the calculation, and $A_c = A_0$ at $r = 0$ is equal to $R_q^{\ 2}$ (i.e., the square of RMS roughness). The height–height correlation function along the first scan direction is given by the following [32]:

$$H_c(r) = \frac{1}{2N_p(N_p - m)} \sum_{j=1}^{N_p} \sum_{i=1}^{N_p - m} \left[h(i+m,j) - h(i,j)\right]^2. \tag{2}$$

All parameters of the Eq. (2) have same meaning as already discussed in above.

Height–height correlation function and autocorrelation function are related by the following [33]:

$$H_c(r) = 2R_q^2\left[1 - A_c(r)\right]. \tag{3}$$

The height–height correlation functions have been computed from AFM images which are shown in Fig. 5.

The value of horizontal distance (r) for which the HHCF increases by a factor (1–1/e) is termed as correlation length [29]. It can also be calculated from ACF. In both cases, the value of correlation length will be same. The values of correlation lengths are 0.41 µm, 0.30 µm, and 0.92 µm, respectively, of IZO/glass, IZO/ITO, and IZO/Si films. The correlation length denotes the spread of the surface fluctuation laterally. However, correlation function defines short range lateral correlation length and beyond that the function starts to oscillate.

Power spectral density (PSD) can be used to understand long-range correlation in rough surface morphology [19]. It is calculated as a first Fourier transformation of surface profile and defined as follows [54]:

$$\mathrm{PSD} = \frac{R_q^2}{2\pi} \int_0^\infty A_c(r) e^{iql} \mathrm{d}r, \tag{4}$$

where the frequency is defined in the range $1/L < q < N_p/2L$ for a $L \times L$-sized image. A relationship between PSD and frequency (q) is established using the scaling concept and given by the following [55]:

$$\mathrm{PSD} \propto q^{-s}, \tag{5}$$

where 's' is defined as the slope of linear fit to PSD log–log plot in Fig. 6. Now, the fractal dimension can be calculated using the following formula [55]:

$$D_f = E_d + \frac{3 - s}{2}, \tag{6}$$

where E_d is Euclidian dimension. The scaling properties of stochastic surfaces can be measured in terms of Hurst exponent [56]. Hurst exponent is calculated as 3-D_f [39]. The

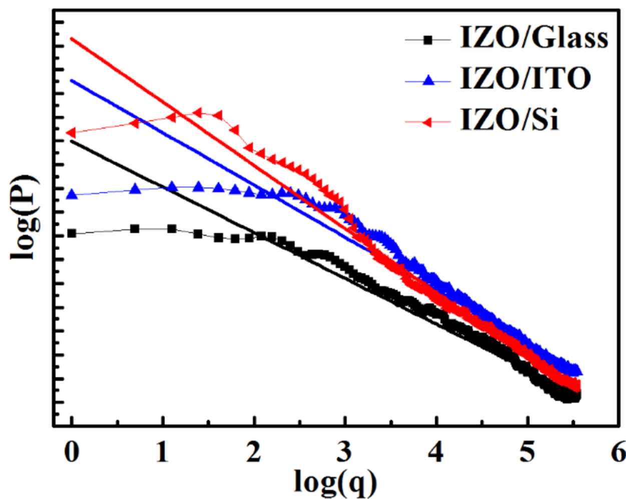

Fig. 6 Power spectral density (P) versus frequency (q) log–log plots calculated from the AFM images of IZO thin films deposited on glass, ITO, and Si substrates

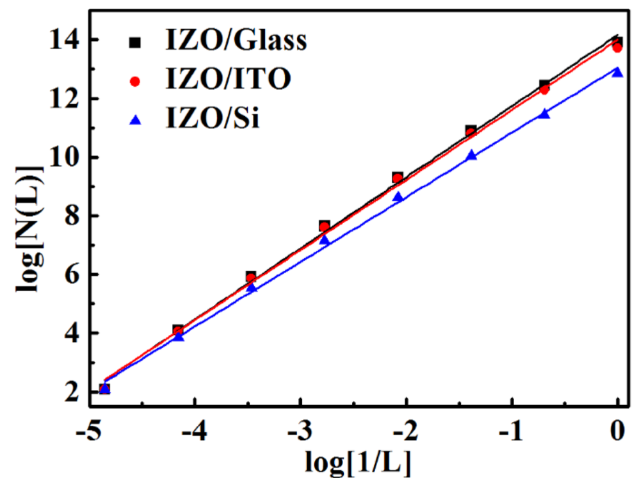

Fig. 7 log [$N(L)$] versus log [$1/L$] plots calculated from AFM images of IZO thin films deposited on glass, ITO, and Si substrates

values of D_f and H of IZO films have been computed and are presented in Table 3.

Fractal dimension is also calculated using square counting method. A fractal object obeys certain power law such as [57]:

$$N(\varepsilon) \sim \varepsilon^{-D_f}, \tag{7}$$

where $N(\varepsilon)$ is the no of features with size ε and D_f is the fractal dimension. The square counting (SC) method is used to find the scaling properties of two-dimensional fractal objects by repeating a measure with square of size ε and counting the number of squares containing atleast one pixel presenting the object under study, $N(\varepsilon)$ [57]:

$$D_f = \lim_{\varepsilon \to 0} \frac{\log N(\varepsilon)}{\log(\varepsilon)}. \tag{8}$$

Thus, the square counting dimension can be calculated from the slope of the log[$N(\varepsilon)$] versus log($1/\varepsilon$) plot, as shown in Fig. 7. Fractal dimension and Hurst exponent values of IZO films have been computed using square counting method and are tabulated in Table 3.

Comparison of the results in Table 3 indicate that D_f and H values calculated from PSD and SC methods are close to each other, and hence, the values are trustable. The values of Hurst exponent quantify different qualities of surface morphology [31]. The values of $H=0.5$, $H>0.5$, and $H<0.5$ indicates respectively, uncorrelated, correlated, and anti-correlated Brownian surfaces [58]. Thus, for IZO/glass film surfaces, the value of H is close to 0.5, and hence, this film surface is not correlated. However, for IZO/ITO films, the value of H increases, and thus, it is a correlated surface. Whereas, for IZO/Si film surfaces, value of H is the highest, and thus, this surface is strongly correlated. Thus, although IZO/Si surface is wrinkled, it has the highest self-similarity. The other two films such as IZO/glass and IZO/ITO have jagged surface morphology and less self similar than IZO/Si films. Thus, the horizontal roughness, i.e., the self-similarity, of a thin-film surface can be quantified precisely with the help of fractal analysis.

Different parts of a surface may not have similar scaling exponent. Therefore, the idea of fractal can be more generalised with the help of multifractal formalism. In this analysis, both local and overall thin-film surface morphoogy could be understood more microscopically and systematically.

Table 3 Fractal dimensions (D_f) and Hurst exponents (H) computed using PSD and square counting (SC) methods from AFM images of In-doped ZnO thin films deposited on glass, ITO, and Si substrates

Sample name	D_f (PSD)	H (PSD)	D_f (SC)	H (SC)
IZO/glass	2.54	0.46	2.42	0.58
IZO/ITO	2.40	0.60	2.39	0.61
IZO/Si	2.16	0.84	2.20	0.80

3.2.2 Multifractal analysis

Fractal models do not characterize spatial anisotropy explicitly. Therefore, the concept of multifractallity has been used to understand mass distribution more microscopically and generalised manner. There are many methodology available to do multifractal analysis. The method of moments or partition function approach has been chosen in this work for its procedural simplicity, accuricy, and widespread use. Mass deposition in local level can be estimated with the help of probability density in the ith square as follows [57]:

$$P_i(\varepsilon) = \frac{N_i(\varepsilon)}{\sum N_i(\varepsilon)}, \tag{9}$$

where $N_i(\varepsilon)$ is the number of pixels containing mass in the ith box of size ε ($\varepsilon \le 1$) and the denominator contains total mass of the system. Lipschitz–Holder exponent α_i and probability density $P_i(\varepsilon)$ scale as follows [59]:

$$P_i(\varepsilon) \sim \varepsilon^{\alpha_i}. \tag{10}$$

If nonlinearity in mass distribution between the squares is absent, then Holder exponent becomes monofractal. A distribution of Holder exponent values could be found in a system. The number of squares $N(\alpha)$ where the probability density P_i has α_i values between α and $\alpha + \mathrm{d}\alpha$ scales as [59–61]:

$$N(\alpha) \sim \varepsilon^{-f(\alpha)}, \tag{11}$$

where $f(\alpha)$ is called multifractallity. Multifractallity can be characterized through the scaling of q th order moments of probability density distributions as follows [60, 62]:

$$Z(q, \varepsilon) = \sum_{i=1}^{N(L)} P_i^q(\varepsilon) = \varepsilon^{(q-1)D_q}, \tag{12}$$

where D_q is generalised fractal dimension. Now, $(q\text{-}1)D_q = \tau(q)$ which is called mass exponent of qth order moment [63, 66]. The mass exponent, $\tau(q)$, can be obtained from the slope of the log–log plot of partition function $Z(q,\varepsilon)$ versus ε. A relationship between mass exponent and multifractallity can be obtained with the help of Legendre transformation [59, 60, 64]:

$$f\left[\alpha(q)\right] = q\alpha(q) - \tau(q) \tag{13}$$

and

$$\alpha(q) = \frac{\mathrm{d}\tau(q)}{\mathrm{d}q}. \tag{14}$$

Square sizes, ε, taken in our computations are 1/256, 1/128,1/64, 1/32, 1/16, 1/8, ¼, ½, and 1. The q range is taken from −5 to +5 with a step of 1. Figure 8 shows that the scaling is good for all q moments and square sizes ε for the IZO/glass films. The partition function versus square size plots for other two films of IZO/ITO and IZO/Si are obtained (not shown here), and they also show good scaling behaviour. Multifractal spectrum has been computed using the slope of these plots, $\tau(q)$. The mass exponents $[\tau(q)]$ have been calculated for different values of moments (q) in a range of $-5 < q < 5$. Figure 9 shows mass exponents as a function of moments for IZO films deposited on glass, ITO, and Si substrates. Careful observation reveals that mass exponent is a nonlinear function of moments. Consequently, there exists multifractallity in IZO film surfaces deposited on glass, ITO, and Si substrates. Multifractal spectra have been calculated using Eqs. (13) and (14). Multifractal spectra of all IZO films are shown in Fig. 10 and multifractal parameters are depicted in Table 4. Thin-film surface morphology can be

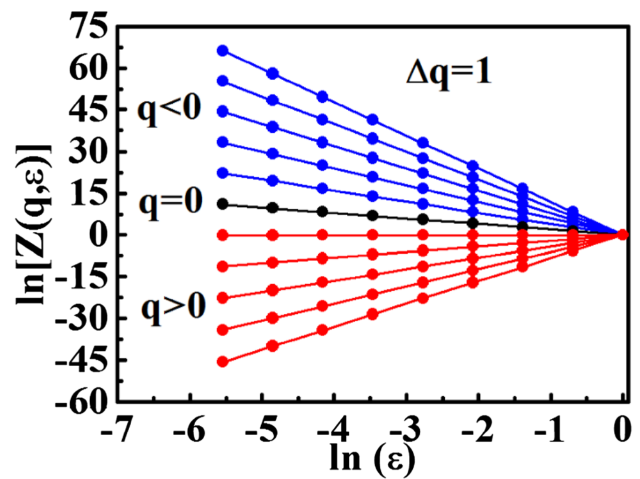

Fig. 8 Plot of $Z(q,\varepsilon)$ for different q values calculated from AFM images of IZO film on glass substrate

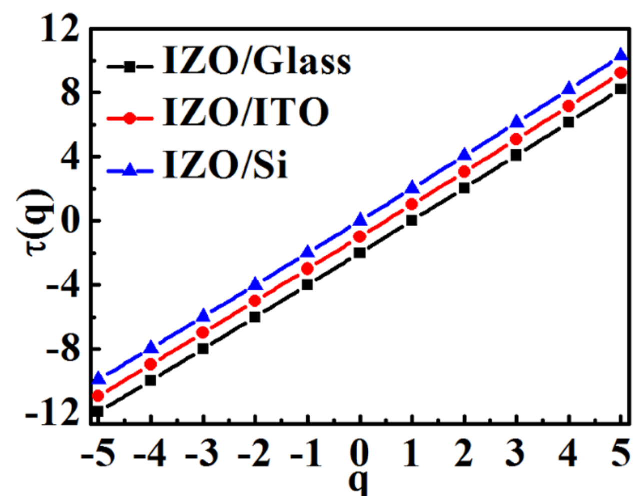

Fig. 9 Mass exponent $\tau(q)$ as a function of q. The curves for IZO/ITO and IZO/Si have been shifted upwards by 1 and 2, respectively, for clarity

described from analysis of this spectrum after extracting the values of $\Delta\alpha$ and Δf [40]. $\Delta\alpha$ signifies the wideness of the probability distribution of mass at the surface, and on the other hand, Δf describes the difference between same size squares throughout the surface [65, 66]. In other words, Δf represents difference of fractal dimensions between maximum and minimum singularity strength [39]. If $\Delta f \to 0$, then height distribution of the deposited mass at highest site is equal to that at the lowest sites [38]. It has been found that Δf values for all films are the same and very small, almost equal to zero. Therefore, all the films deposited on glass, ITO, and Si substrate have equal number of peaks and valleys. It is noteworthy to mention that the conventional statistical analysis do not provide this information with such a precision.

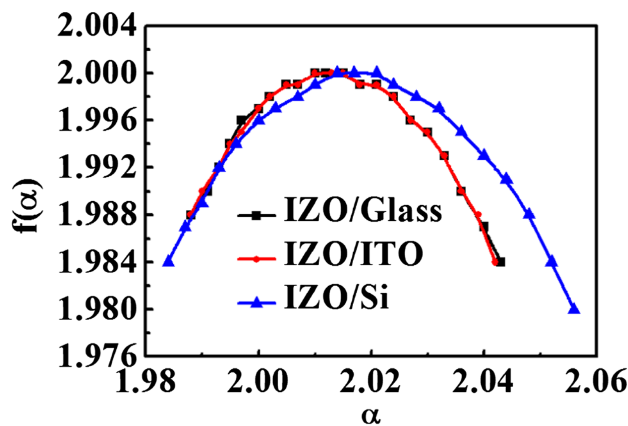

Fig. 10 Multifractal spectra [$f(\alpha)$ versus α] for AFM images of IZO films deposited on glass, ITO, and Si substrates

Table 4 Multifractal parameters computed from AFM images of In-doped ZnO thin films deposited on glass, ITO, and Si substrates

Sample name	$\Delta\alpha$	Δf
IZO/glass	0.055	0.004
IZO/ITO	0.054	0.004
IZO/Si	0.072	0.004

The strength of multifractallity could be better described in the present case by the width of the multifractal spectrum, $\Delta\alpha$. It is clear from Table 4 that the value of $\Delta\alpha$, i.e., the width of the singularity spectrum, is the highest for the films deposited on Si substrates. It is the lowest and almost equal in films deposited on glass and ITO substrates. Thus, IZO thin films deposited on Si substrates are more vertically irregular or rough as, in these films, there exist larger difference between the highest and lowest growth probability of the surface, Whereas the films deposited on glass and ITO have almost similar kind of growth.

It is noteworthy to mention that an explicit statistical description cannot be extracted from the conventional statistical analysis of a film surface in a scale-independent manner. Thus, the present work discloses the opportunity to describe surface morphology of wide band-gap oxide multifunctional thin films in more detailed, precise, and independent manner which could be used in future works to correlate fractal and multifractal parameters with various physical properties.

4 Conclusion

Indium-doped ZnO thin films have been deposited on glass, ITO, and Si substrates via sol–gel spin coating method. GIXRD patterns analysis show highest average crystallite size and residual stress in IZO/Si films, whereas lowest average crystallite size has been observed in IZO/glass films with moderate residual stress. Lowest residual stress is found in IZO/ITO films. First-order statistical analysis shows that the IZO/Si films have highest vertical roughness, whereas IZO/ITO has lower roughness than IZO/Si. IZO/glass has the lowest vertical roughness and surface symmetry among all. Self-similarities in surfaces having different surface texture and interface width could not be understood with the help of the conventional first-order statistical parameters. Therefore, height distribution is correlated, and consequently, fractal behaviour of the film surfaces has been studied. Analysis of fractal parameters reveals that, despite of wrinkled surface formation with the highest vertical roughness in IZO/Si films, spatial self-similarity is the highest for these films. To assess inhomogeneity in scaling exponents, multifractal analysis is done. More prominant multifractallity in IZO/Si films has been observed than in IZO/ITO and IZO/glass films. Thus, height distribution of IZO/Si films is the widest as the highest and lowest growth probability of the surface has large difference. Multifractal behaviour of IZO/ITO and IZO/glass films is almost similar.

Therefore, surface growth and its corresponding physical and tribological properties during micro- and nanofabrication could be understood in further detailed and independent manner with the help of fractal and multifractal formalism. Thus, understanding the fractal and multifractal features of the surface morphology may become highly useful in the fabrication and prediction of thin films for application in TCO materials, sensors, water-repellent surfaces, etc.

Acknowledgements Author KG thanks UGC, India, for providing fellowship to carry out this research work. Both authors are thankful to Department of Pure and Applied Physics, Guru Ghasidas Vishwavidyalaya, Bilaspur, India, for providing synthesis and characterization facilities.

References

1. U. Ozgur, D. Hofstetter, H. Morkoc, ZnO devices and applications: a review of current status and future prospects. Proc. IEEE **98**(**7**), 1255–1268 (2010)
2. J. Lu, Z. Shi, Y. Wang, Y. Lin, Q. Zhu, Z. Tian, J. Dai, S. Wang, C. Xu, Plasmon-enhanced electrically light-emitting from ZnO nanorod arrays/p-GaN heterostructure devices. Sci. Rep **6**, 25645 (2016)
3. M. Hussain, M.A. Abbasi, A. Khan, O. Nur, M. Willander, Comparative study of energy harvesting from ZnO nanorods using different flexible substrates. Energy Harvest. Syst. **1–2**, 19–26 (2014)
4. E. Muchuweni, T.S. Sathiaraj, H. Nyakotyo, Synthesis and characterization of zinc oxide thin films for optoelectronic applications. Heliyon **3**, e00285 (2017)
5. V. Balaprakash, P. Gowrisankar, S. Sudha, R. Rajkumar, Aluminum doped ZnO transparent conducting thin films prepared by sol-gel dip coating technique for solar cells and optoelectronic applications. Mater. Technol. **33**(6), 414–420 (2018)
6. Q. Boyer, S. Duluard, C. Tenailleau, F. Ansart, V. Turq, J.P. Bonino, Functionalized superhydrophobic coatings with micro-/

nanostructured ZnO particles in a sol–gel matrix. J. Mater. Sci. **52**, 12677–12688 (2017)
7. N. Mufti, D. Arista, M. Diantoro, A. Fuad, A. Taufiq, Sunaryono, the effect of thickness of ZnO thin films on hydrophobic self-cleaning properties. IOP Conf. Ser. Mater. Sci. Eng. **202**, 012006 (2017)
8. A.J. Mughal, B. Carberry, J.S. Speck, S. Nakamura, S.P. Denbaars, Structural and optical properties of group III doped hydrothermal ZnO thin films. J. Electron. Mater. **46**(3), 1821–1825 (2017)
9. B. Paul, B. Singh, S. Ghosh, A. Roy, A comparative study on electrical and optical properties of group III (Al, Ga, In) doped ZnO. Thin Solid Films **603**, 21–28 (2016)
10. A. Hafdallah, F. Yanineb, M.S. Aida, N. Attaf, In doped ZnO thin films. J. Alloys Compd. **509**, 7267–7270 (2011)
11. E. Lunaarredondoa, A. Maldonadoa, R. Asomozaa, D.R. Acostab, M. Melendezlirac, M. Delalolvera. Indium-doped ZnO thin films deposited by the sol–gel technique. Thin Solid Films **490**, 132–136 (2005)
12. H. Sun, S.-U. Jen, S.-C. Chen, S.-S. Ye, X. Wang, The electrical stability of In-doped ZnO thin films deposited by RF sputtering. J. Phys. D Appl. Phys. **50**, 045102 (2017)
13. M. Yamamoto, N. Nishikawa, H. Mayama, Y. Nonomura, S. Yokojima, S. Nakamura, K. Uchida, Theoretical explanation of the lotus effect: superhydrophobic property changes by removal of nanostructures from the surface of a lotus leaf. Langmuir **31**(26), 7355–7363 (2015)
14. S.S. Latthe, C. Terashima, K. Nakata, A. Fujishima, Superhydrophobic surfaces developed by mimicking hierarchical surface morphology of lotus leaf. Molecules **19**, 4256–4283 (2014)
15. G. Hübschen, I. Altpeter, R. Tschuncky, H.-G. Herrmann, *Materials Characterization Using Nondestructive Evaluation (NDE) Methods* (Woodhead Publishing, New York, 2016)
16. P. Hall, S. Davies, On direction-invariance of fractal dimension on a surface. Appl. Phys. A **60**, 271–274 (1995)
17. Y.R. Jeng, P.C. Tsai, T.H. Fang, Nanomeasurement and fractal analysis of PZT ferroelectric thin films by atomic force microscopy. Microelectron. Eng. **65**, 406 (2003)
18. A. Mannelqvist, M.R. Groth, Comparison of fractal analyses methods and fractal dimension for pre-treated stainless steel surfaces and the correlation to adhesive joint strength. Appl. Phys. A **73**, 347–355 (2001)
19. D. Raoufi, Fractal analyses of ITO thin films: a study based on power spectral density. Phys. B **405**, 451–455 (2010)
20. D. Dallaeva, S. Talu, S. Stach, P. Skarvada, P. Tomanek, L. Grmela, AFM imaging and fractal analysis of surface roughness of AlN epilayers on sapphire substrates. Appl. Surf. Sci. **312**, 81–86 (2014)
21. L. Chen, J. Xu, P. Fleming, J.D. Holmes, M.A. Morris, Dynamic stable nanostructured metal oxide fractal films grown on flat substrates. J. Phys. Chem. C **112**, 14286–14291 (2008)
22. J. Arjomandi, D. Raoufi, F. Ghamari, Surface characterization and morphology of conducting polypyrrole thin films during polymer growth on ITO glass electrode. J. Phys. Chem. C **120**(32), 18055–18065 (2016)
23. N. Xie, W. Shao, L. Feng, L. Lv, L. Zhen, Fractal analysis of disordered conductor–insulator composites with different conductor backbone structures near percolation threshold. J. Phys. Chem. C **116**, 19517–19525 (2012)
24. Z. Chen, D. Pan, B. Zhao, G. Ding, Z. Jiao, M. Wu, C.-H. Shek, C.M.L. Wu, J.K.L. Lai, Insight on fractal assessment strategies for tin dioxide thin films. ACS Nano **4**(2), 1202–1208 (2010)
25. N. Saxena, T. Naik, S. Paria, Organization of SiO_2 and TiO_2 nanoparticles into fractal patterns on glass surface for the generation of superhydrophilicity. J. Phys. Chem. C **121**(4), 2428–2436 (2017)
26. H. Awada, B. Grignard, C. Jerome, A. Vaillant, J.D. Coninck, B. Nysten, A.M. Jonas, Correlation between superhydrophobicity and the power spectral density of randomly rough surfaces. Langmuir **26**(23), 17798–17803 (2010)
27. R. Jain, R. Pitchumani, Fractal model for wettability of rough surfaces. Langmuir **33**, 7181–7190 (2017)
28. U.B. Singh, R.P. Yadav, R.K. Pandey, D.C. Agarwal, C. Pannu, A.K. Mittal, Insight mechanisms of surface structuring and wettability of ion treated Ag thin films. J. Phys. Chem. C **120**(10), 5755–5763 (2016)
29. R.P. Yadav, M. Kumar, A.K. Mittal, S. Dwivedi, A.C. Pandey, On the scaling law analysis of nanodimensional LiF thin film surfaces. Mater. Lett. **126**, 123–125 (2014)
30. Ş Ţălu, R.P. Yadav, A.K. Mittal, A. Achour, C. Luna, M. Mardani, S. Solaymani, A. Arman, F. Hafezi, A. Ahmadpourian, S. Naderi, K. Saghi, A. Méndez, G. Trejo, Application of Mie theory and fractal models to determine the optical and surface roughness of Ag–Cu thin films. Opt Quant Electron **49**, 256 (2017)
31. R.P. Yadav, D.C. Agarwal, M. Kumar, P. Rajput, D.S. Tomar, S.N. Pandey, P.K. Priya, A.K. Mittal, Effect of angle of deposition on the Fractal properties of ZnO thin film surface. Appl. Surf. Sci. **416**, 51–58 (2017)
32. R.P. Yadav, T. Kumar, A.K. Mittal, S. Dwivedi, D. Kanjilal, Fractal characterization of the silicon surfaces produced by ion beam irradiation of varying fluences. Appl. Surf. Sci. **347**, 706–712 (2015)
33. U.B. Singh, R.P. Yadav, R. Kumar, S. Ojha, A.K. Mittal, S. Ghosh, F. Singh, Nanostructuring and wettability of ion treated Au thin films. J. Appl. Phys **122**, 185303 (2017)
34. R.P. Yadav, U.B. Singh, A.K. Mittal, S. Dwivedi, Investigating the nanostructured gold thin films using the multifractal analysis. Appl. Phys. A **117**, 2159–2166 (2014)
35. R.P. Yadav, M. Kumar, A.K. Mittal, A.C. Pandey, Fractal and multifractal characteristics of swift heavy ion induced self-affine nanostructured BaF2 thin film surfaces. Chaos **25**, 083115 (2015)
36. R.P. Yadav, R.K. Pandey, A.K. Mittal, S. Dwivedi, A.C. Pandey, Multifractal analysis of sputtered CaF2 thin films. Surf. Interface Anal. **45**, 1775–1780 (2013)
37. S. Hosseinabadi, F. Abrinaei, M. Shirazi, Statistical and fractal features of nanocrystalline AZO thin films. Phys. A **481**, 11–22 (2017)
38. M. Nasehnejad, M.G. Shahraki, G. Nabiyouni, Atomic force microscopy study, kinetic roughening and multifractal analysis of electrodeposited silver films. Appl. Surf. Sci. **389**, 735–741 (2016)
39. R.P. Yadava, S. Dwivedi, A.K. Mittal, M. Kumar, A.C. Pandey, Fractal and multifractal analysis of LiF thin film surface. Appl. Surf. Sci. **261**, 547–553 (2012)
40. R.P. Yadav, S. Dwivedi, A.K. Mittal, M. Kumar, A.C. Pandey, Analyzing the LiF thin films deposited at different substrate temperatures using multifractal technique. Thin Solid Films **562**, 126–131 (2014)
41. International Centre of Diffraction Data, Powder Diffraction File, JCPDS File No 00-036-1451 (1996)
42. G.K. Williamson, W.H. Hall, X-ray line broadening from filed aluminium and wolfram. Acta Metall. **1**, 22 (1953)
43. R.K. Pandey, K. Ghosh, S. Mishra, J.P. Bange, P.K. Bajpai, D.K. Gautam, Effect of film thickness on structural and optical properties of sol–gel spin coated aluminum doped zinc oxide (Al:ZnO) thin films. Mater. Res. Express **5**(8), 086408 (2018)
44. G.A. Kumar, M.V.R. Reddy, K.N. Reddy, Structural and optical properties ZnO thin films grown on various substrates by RF magnetron sputtering. IOP Conf. Ser. Mater. Sci. Eng. **73**, 012133 (2015)
45. W. Chebil, A. Fouzri, B. Azeza, N. Sakly, R. Mghaieth, A. Lusson, V. Sallet, Influence of substrate on structural, morphological and optical properties of ZnO films grown by SILAR method. Bull. Mater. Sci. **37**(6), 1283–1291 (2014)

46. V. Craciun, D. Craciun, X. Wang, T.J. Anderson, R.K. Singh, Transparent and conducting indium tin oxide thin films grown by pulsed laser deposition at low temperatures. J. Optoelectron. Adv. M. **5**(2), 401–408 (2003)
47. I. Ozena, M.A. Gulgun, Residual stress relaxation and microstructure in ZnO thin films. Adv Sci Tech. **45**, 1316–1321 (2006)
48. N. Bowden, S. Brittain, A.G. Evans, J.W. Hutchinson, G.M. Whitesides, Spontaneous formation of ordered structures in thin films of metals supported on an elastomeric polymer. Nature **393**, 146–149 (1998)
49. S.J. Kwon, J.-H. Park, J.-G. Park, Wrinkling of a sol-gel-derived thin film. Phys. Rev. E **71**, 011604 (2005)
50. R. Shivanna, S. Rajaram, K.S. Narayan, Interface engineering for efficient fullerene-free organic solar cells. Appl. Phys. Lett. **106**, 123301 (2015)
51. M. Rapso, Q. Ferreira, P.A. Ribeiro, A Guide for Atomic Force Microscopy Analysis of soft-condensed Matter (Modern Research and Educational Topics in Microscopy). ed A. Merdez-Vilas et al. (Formatex Spain, 2010) p 758
52. R. Mohammadigharehbagh, S. Pat, S. Ozen, H.H. Yudar, S. Korkmaz, Investigation of the optical properties of the indium-doped ZnO thin films deposited by a thermionic vacuum arc. Optik **157**, 667–674 (2018)
53. Y. Zhao, G. Ching, T. Wang, M. Lu, *Characterization of Amorphous and Crystalline Rough Surface: Principle and Applications* (Academic Press, New York, 2001)
54. M. Pelliccione, T.-M. Lu, *Evolution of Thin Film Morphology Modeling and Simulations* (Springer, New York, 2008)
55. M.B. Khamesee, Y. Kurosaki, M. Matsui, K. Murai, Nanofractal analysis of material surfaces using atomic force microscopy. Mater. Trans. **45**(2), 469 (2004)
56. B.B. Mandelbrot, J.W. Van Ness, Fractional brownian motions, fractional noises and applications. SIAM Rev. **4**, 422 (1968)
57. A.N.D. Posadas, D. Gimenez, R. Quiroz, R. Protz, Multifractal characterization of soil pore systems. Soil Sci. Soc. Am. J. **67**, 1361–1369 (2003)
58. A. Carbone, Algorithm to estimate the Hurst exponent of high-dimensional fractals. Phys. Rev. E **76**, 056703 (2007)
59. T.C. Halsey, M.H. Jensen, L.P. Kadanoff, I. Procaccia, B.I. Shraiman, Fractal measures and their singularities: the characterization of strange sets. Phys. Rev. A **33**, 1141 (1986)
60. A.B. Chhabra, C. Meneveu, R.V. Jensen, K.R. Sreenivasan, Direct determination of the f(α) singularity spectrum and its application to fully developed turbulence. Phys. Rev. A **40**, 5284 (1989)
61. A.B. Chhabra, R.V. Jensen, Direct determination of the f(α) singularity spectrum. Phys. Rev. Lett. **62**, 1327 (1989)
62. G. Korvin, *Fractal Methods in the Earth Science* (Elsevier, Amsterdam, 1992)
63. T. Vicsek, *Fractal Growth Phenomena*, 2nd edn. (Word Scientific Publishing Co., Singapore, 1992)
64. H.B. Callen, *Thermodynamics and an Introduction to Thermo-Statistics*, 2nd edn. (John Wiley & Sons, New York, 1985)
65. Z.W. Chen, J.K.L. Lai, C.H. Shek, Multifractal spectra of scanning electron microscope images of SnO_2 thin films prepared by pulsed laser deposition. Phys. Lett. A. **345**, 218–223 (2005)
66. D. Raoufi, H.R. Fallah, A. Kiasatpour, A.S.H. Rozatian, Multifractal analysis of ITO thin films prepared by electron beam deposition method. Appl. Surf. Sci. **254**, 2168–2173 (2008)